Robotica (2013) volume 31, pp. 89–98. © Cambridge University Press 2012
doi:10.1017/S0263574712000112

A fast mesoscale quadruped robot using piezocomposite actuators

Thanhtam Ho and Sangyoon Lee*

Department of Mechanical Design and Production Engineering Konkuk University, 1 Hwayang-dong, Gwangjin-gu, Seoul, Korea, 143-701

(Accepted March 2, 2012. First published online: April 4, 2012)

SUMMARY

This paper introduces the design, analysis, and experimental results of a fast mesoscale (12 cm length) quadruped mobile robot that employs unconventional actuators. Four legs of the robot are actuated by two pieces of piezocomposite actuator named LIPCA, which enables the robot to achieve the bounding gait with only one degree of freedom per leg. The forward locomotion is obtained by a creative idea in the design and the speed can be controlled by changing the frequency of actuators. The mechanism of power transfer has been improved in order to use the actuation power more efficiently. Two small RC-servo motors are added to control the locomotion direction. In addition, a small power supply and control circuit is developed that is fit for the robot. Our experiments show that the robot can locomote as fast as about two times its body length per second with the circuit board and a battery installed. The robot is also able to change the heading direction in a controlled way and is capable of continuous operation for 35 min.

KEYWORDS: Legged robot; Piezocomposite actuator; Bounding locomotion.

1. Introduction

Mobile robots have drawn enormous attention from robot engineers and scientists as well as the general public in recent years. Most mobile robots employ either wheels or legs as the means of locomotion. Legged robots are known to be advantageous over wheeled ones in terms of the mobility and obstacle-avoiding ability [1–4]. It is natural that legged robot designs often employ the structure and function of biological creatures. The biomimetic designs can be classified into two categories. The robots in the first category are the result of attempt to mimic animals or insects as closely as possible. The robot mechanisms need many DOF (degree of freedom) and the locomotion entails a complex control algorithm. The robots of this type are often developed using conventional actuators such as electromagnetic motors and hydraulic or pneumatic actuators. Some representative robots in this group are 32-DOF cockroach robot named Ajax [5], a rough-terrain robot BigDog [6], and a quadruped robot Tekken [7]. Though such robots show remarkably agile maneuverability and mobility on many types of terrain, complex mechanisms result in large size and heavy weight. Tekken, for example, is capable of various locomotion gaits including walk, trot, and bound, but the robot mechanism without the controller hardware weighs at about 31 kg. Other legged robots that can be classified to this category are Sprawlita [8] and RHex [9]. Compared to Ajax, BigDog, or Tekken, the structures of Sprawlita and RHex are simplified to some extent but they are still complex and heavy.

The main characteristics of robots in the second category are their small size and simple mechanism. Few ideas of biomimetics are directly reflected on the design of the robots. Agility in the motion is not usually an attribute of these robots. However their strength lies in the size and the weight. Another distinctive feature of these robots is the use of unconventional actuators, for example, piezoelectric materials, shape memory alloy (SMA), electroelastomer.

Goldfarb and his coworkers introduced a mesoscale legged robot driven by piezoelectric actuators [10]. The robot is 9 cm long and employs the trotting gait. The robot can change the locomotion direction by changing the frequency of voltage that is applied to the actuators. Another piezoelectrically actuated legged robot is the 3 g crawling robot [11]. This self-contained hexapod with 35 mm length is designed to move in the alternating tripod gait driven by two piezoelectric actuators. The robot shows the advantage in reducing the size of biomimetic robot.

SMA has also been used as the actuation source of legged robots. One example is RoACH, the 2.4 g crawling robot actuated by SMA actuators [12]. The small robot made of glass-reinforced composites and flexible polymer can achieve the speed of one body length per second or 3 cm/s in the untethered operation.

In case of MERbot [13], another type of unconventional actuator named electroelastomer roll actuator is used. MERbot is a hexapod whose legs are 2-DOF spring electroelastomer roll actuator. The robot structure is simple with a hexagonal frame, legs, and wires. The robot with 292 g weight is able to perform the dual tripod gait at the speed of two-thirds its body length per second or 13.6 cm/s with an external power supply.

The legged robots using such unconventional actuators are usually smaller and lighter than ones in the first category, but they are slow and can move in only one specific locomotion gait. Changing the locomotion gait to alter the speed or the direction is quite difficult in this case because the number of controllable actuators is minimized.

In this paper, we present a fast mesoscale (12 cm length) quadruped robot that combines the strengths of the aforementioned robot categories. Four legs of the robot are actuated by a kind of piezocomposite actuator, LIPCA,

* Corresponding author. E-mail: slee@konkuk.ac.kr

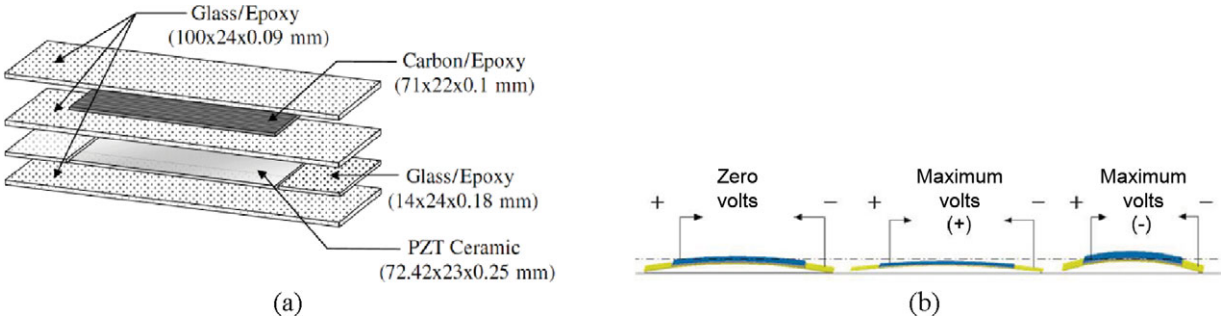

Fig. 1. (Colour online) LIPCA-C2: (a) Structure of LIPCA-C2. (b) Vertical vibration of LIPCA [16].

(lightweight piezoceramic composite curved actuator) [14]. Two pieces of LIPCA are used to enable the robot to accomplish the bounding gait with only one DOF per leg.

2. Design of the Robot

2.1. LIPCA actuator

LIPCA is a piezocomposite actuator that is composed of a piezoelectric ceramic layer and layers of glass/epoxy and carbon/epoxy. The structure is illustrated in Fig. 1(a). The piezoelectric ceramic film is the most essential part for generating the vertical displacement of LIPCA. When a square voltage signal is applied to the terminals of a LIPCA piece, it starts the vibration around the neutral position (see Fig. 1(b)). Several versions of LIPCA have been developed. LIPCA-C2 was chosen among them for our robot actuator because experimental results show that it can generate a larger displacement than the other LIPCA versions [15]. Compared to the previous version such as LIPCA-C1, the displacement of LIPCA-C2 is improved by about 170%. This result was obtained by changing the lay-up structure of LIPCA, which causes the position of neutral axis to move outside of the PZT wafer [15].

LIPCA possesses several characteristics which are useful to be the actuator for mesoscale legged robots. First, LIPCA is a linear actuator, and so well-suited to implement the motion of leg. Second, LIPCA is a light actuator, which is a desirable attribute for mesoscale robots. Third, LIPCA has a higher force and a larger displacement than other piezocomposite actuators. It is verified by experiments that the displacement of LIPCA-C2 is about 13% larger than that of THUNDER 7-R-24w [16], while LIPCA-C2 is about 34% lighter than THUNDER [17].

When the applied voltage is 400 Vpp with the frequency of 1.0 Hz, the displacement of LIPCA-C2 is about 1.155 mm. However the displacement can be raised to 1.5 mm at the resonant frequency condition of our robot. The locomotion speed of our robot depending on the frequency of applied voltage is described in Section 4.2.

2.2. Design concept of robot

The design concept of our legged robot can be summarized to the minimization of two aspects: the number of DOF per leg and the number of actuators. Since the constraints in the size and weight of robot are relatively large when using piezocomposite actuators, the importance of a simple structure is significant. Such issues were also considered in the development of our previous quadruped robot [18], which, however, had weakness in the locomotion speed and the direction control.

The overall design of our new robot is shown in Fig. 2. Like the previous version, four legs of the quadruped are driven by two pieces of LIPCA and each leg possesses only one

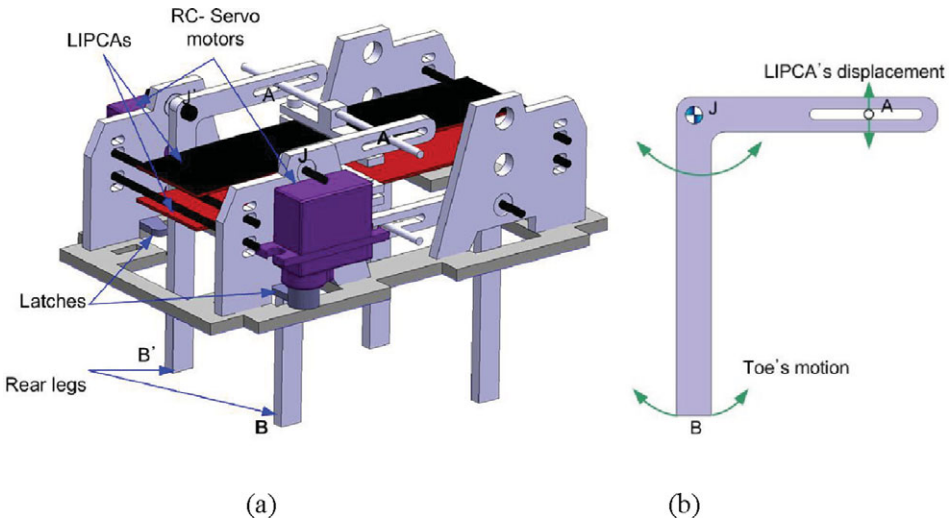

Fig. 2. (Colour online) Design of the robot body and leg: (a) Overall design of the robot. (b) Gamma-shaped leg.

https://doi.org/10.1017/S0263574712000112 Published online by Cambridge University Press

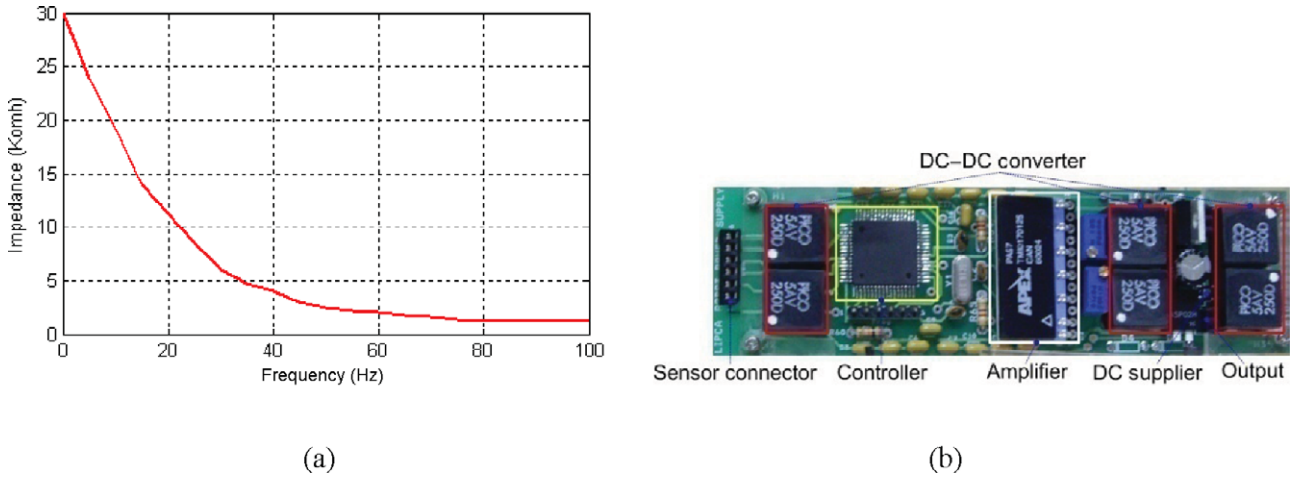

Fig. 3. (Colour online) Development of a power supply and control circuit board: (a) Impedance characteristic of LIPCA. (b) Power supply and control circuit board.

DOF. However, the design of robot leg and link mechanism has been improved. The two rear legs are connected directly to the upper LIPCA and the two front legs are actuated by the bottom LIPCA. Each leg has a gamma shape and employs a simple crank mechanism. Every leg is attached to the body frame by a revolute joint that is set at the corner of the leg (the hip joint at the point J in Fig. 2(b)). The terminal A of the leg in Fig. 2(a) is connected directly to the upper LIPCA piece and the other terminal is at the leg toe (point B). Compared to the design of previous version [18], the motion of LIPCA is now transferred directly to the robot legs, and hence the power loss is minimized.

As shown in Fig. 2(a), two LIPCA pieces are placed in layers perpendicular to the robot legs. Both ends of LIPCA are fixed to the body frame and the vibration occurs in the middle line of LIPCA (line AA' in Fig. 2(a)), which is based on the fact that LIPCA produces the largest displacement in the middle line [15]. The vibration of LIPCA is generated in the vertical direction and this motion is transferred to the robot legs. As shown in Fig. 2(b), the vertical motion from LIPCA causes the leg to rotate around the hip joint J, and the toe of each leg therefore obtains the back and forth motion. Notice that two RC-servo motors are attached to the body frame to control the direction of locomotion. The direction control method of the robot is presented in Section 3.3.

2.3. Power and control electronics

In addition to the mechanical part, the power supply and control circuit is another significant part for autonomous mobile robots. In case of our robot, the characteristics of LIPCA have a large effect on the design of the circuit. Unlike conventional actuators, the piezocomposite actuator LIPCA requires very high voltage for its operation. Experimental results show that LIPCA performs the best when the applied voltage is about 400 V peak-to-peak [16]. Hence, the power supply for the quadruped robot has to produce such a high voltage as LIPCA requires. Here our proposed solution is using a DC–DC converter chip named PICO 5AV250D. The converter chip can generate dual ±250 V from 5V input source. Compared to other power solutions for piezoelectric actuators such as the hybrid boost converter with a cascaded charge pump used in Microbots [19], this method can provide a simple, light, and stable circuit.

Another design factor that stems from the characteristics of LIPCA is the impedance of LIPCA. Our experiments on the electronic characteristic of LIPCA show that the impedance of LIPCA is similar to that of a capacitor. Figure 3(a) shows that the relation of LIPCA impedance and the frequency of applied voltage. As the frequency increases the impedance decreases. In particular the impedance falls down significantly in the range of 20 Hz to 50 Hz where the robot is supposed to operate well. Though LIPCA works better at such frequencies, its impedance is low while the applied voltage is still kept high and the current required is quite large too.

Increasing the current causes the overloading in the PICO chip. One general solution to the problem is using large internal resistance of the circuit. However, a problem occurs when the internal resistance is combined with the capacitive impedance characteristic of LIPCA. The combination forms an RC circuit which distorts the square signal generated by the circuit, and hence LIPCA may not work properly. In order to overcome the problem, six PICO chips are connected parallel in our circuit as shown in Fig. 3(b), and hence the current is increased six times. The power circuit board also works as the control circuit for the robot. An ATmega128 microcontroller is incorporated in the board to generate a square signal driving the amplifier chip APEX PA97. The servo motors which activate the latches are also controlled by the microcontroller. An Analog-to-Digital module embedded on the microcontroller can be used to get data from other devices, for example, range sensors that can be useful for avoiding obstacles.

3. Motion Control of the Robot

This section presents how the robot can execute two types of motion: straight-line locomotion and turning. In the former motion, only LIPCA actuators are utilized, while both LIPCA and servos are employed during turning.

https://doi.org/10.1017/S0263574712000112 Published online by Cambridge University Press

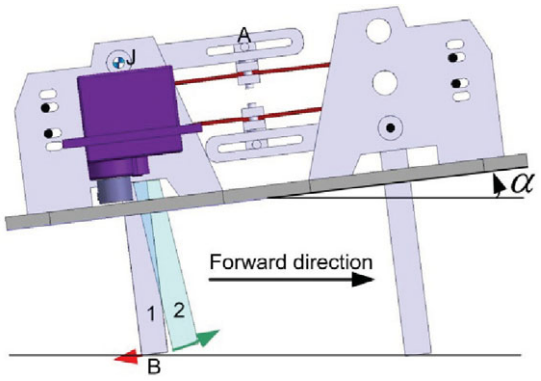

Fig. 4. (Colour online) Forward locomotion and the body slope angle alpha.

3.1. *Forward locomotion generation and bounding gait*

The simplicity of mechanical structure design can result in a significant reduction in the size and weight of robot. However, it entails more difficulty in the control of robot to achieve a desired locomotion gait successfully. Each leg of legged robots usually has three DOF or more: one or more DOF are for lifting the leg while the others for swinging (Ajax [5] is one example). However, our robot has only one DOF per leg, and hence a different control approach is required.

One of the first successful control methods for robots with one DOF per leg can be found in Scout robots [20]. In Scout 1 robot [21], the hip angles and the angular velocities are controlled to obtain a rocking-like walking gait. The ground clearance is produced by the body pitching, and it enables the leg to swing. This method is quite simple and reasonable but it is considered unsuitable for our robot because of the characteristic of LIPCA actuator. LIPCA possesses a bang–bang-like behavior: it switches between the highest position and the lowest one when an electric voltage is applied. That is, intermediate positions cannot be obtained. As a result, we cannot control the rotation angle of the robot leg exactly. Our robot may be considered as a binary-actuation robot, in which sense it has a similarity with Zhou's model of rigid-link binary walking robot [22]. However, compared to our robot model, Zhou's model has many different points, in particular the number of DOF per leg.

Instead, we present a simple solution to overcome the problem and realize the forward locomotion: making a difference between the front leg length and the rear one, as illustrated in Fig. 4. Notice the motion of the rear legs in Fig. 4. When the robot is walking, the rear legs can take two positions. The position 1 corresponds to the case where the LIPCA pieces move down and the position 2 is obtained when they move up. When the leg moves from the position 1 to 2, the toe does not contact the ground due to the body slope angle alpha. This behavior is similar to lifting the leg up off the ground. When the leg moves back to the position 1, the toe contacts the ground and is able to generate a pushing force, which enables the robot to move forward.

For the locomotion gait of our robot, we chose the bounding gait, where the front legs form a pair and the rear ones make another pair and the pairs move alternately. The bounding gait is suitable for our design because two LIPCA pieces are adequate for two pairs of legs and driving the four legs. It was also found to have an advantage over the trotting gait in terms of the locomotion speed because the trotting gait required a more complex mechanism and a heavier and less efficient structure [23]. In our robot, two LIPCA pieces are driven by two square signals which have the same frequency and amplitude but in the opposite phases.

The bounding gait provides an important feature in the robot structure: symmetry of the locomotion mechanism. Both rear legs move almost equally in the manner, time, and distance because they are driven by the same LIPCA piece. The same mechanism occurs for the front legs. Due to the symmetry, the robot can continue the locomotion even when one LIPCA piece fails, the experimental results of which are described in Section 4.2. This feature cannot be obtained in the trotting gait [10]. Another important feature of the bounding gait is that it is a dynamically stable gait because each pair of legs supports the robot alternately during the bounding motion. The dynamical stability can increase the locomotion speed of the robot dramatically [4].

3.2. *Dynamics analysis*

Although the dynamics model is not used further in the current work, it should be useful for developing control algorithms for such robots as ours. We assume in this discussion that the robot legs are rigid and weightless and they do not slip on the floor. In the typical bounding gait, which can be found in a bounding robot SCAMPER [24], one standing phase (standing on the rear or front legs) is followed by one flying phase. However in our LIPCA robot, the LIPCA actuator is not powerful enough to produce the flying phase. In fact, as illustrated in Fig. 5, the robot stands on the rear legs in the first phase called the rear leg standing phase. Then both legs touch the floor and especially the front legs impact on the floor (front leg falling phase). In the next phase, the robot stands on the front legs (front leg standing phase). Then the rear leg falling phase is followed. Compared to the standing phases, the falling phases occur in a much shorter time.

The dynamics model for each phase is built using the Lagrange's equation. In the first phase, the front leg is taken off the floor and the robot body is supported by the rear legs only. Since the mass of the front leg is neglected and the robot does not slip on the floor, the robot can be modeled as a two-DOF inverted pendulum (see the fist model in Fig. 5). In Fig. 5, M is the center of robot body and the center of rotation is the point B. In the figure, l_r is the length of rear leg, α is the slope angle of robot body, u_r is the displacement of LIPCA, and JM, θ_{ro}, d are geometrical parameters. In order to simplify the expressions, we introduce temporary variables: $L_r = JM$, $q_1 = \alpha + \frac{u_r}{d}$, $q_2 = \alpha + \theta_{r0}$.

Using the Lagrange's equation for the two-DOF inverted pendulum, the two dynamics equations of the robot in the first phase can be derived as under:

$$\begin{cases} ml_r^2\ddot{q}_1 + ml_rL_r\ddot{q}_2\sin(q_2-q_1) \\ \quad + ml_rL_r\dot{q}_2^2\cos(q_2-q_1) - mgl_r\sin q_1 = \tau_r \\ ml_rL_r\ddot{q}_1\sin(q_2-q_1) + (mL_r^2 + J_r)\ddot{q}_2 \\ \quad - ml_rL_r\dot{q}_1^2\cos(q_2-q_1) + mgL_r\cos q_2 = 0. \end{cases} \quad (1)$$

https://doi.org/10.1017/S0263574712000112 Published online by Cambridge University Press

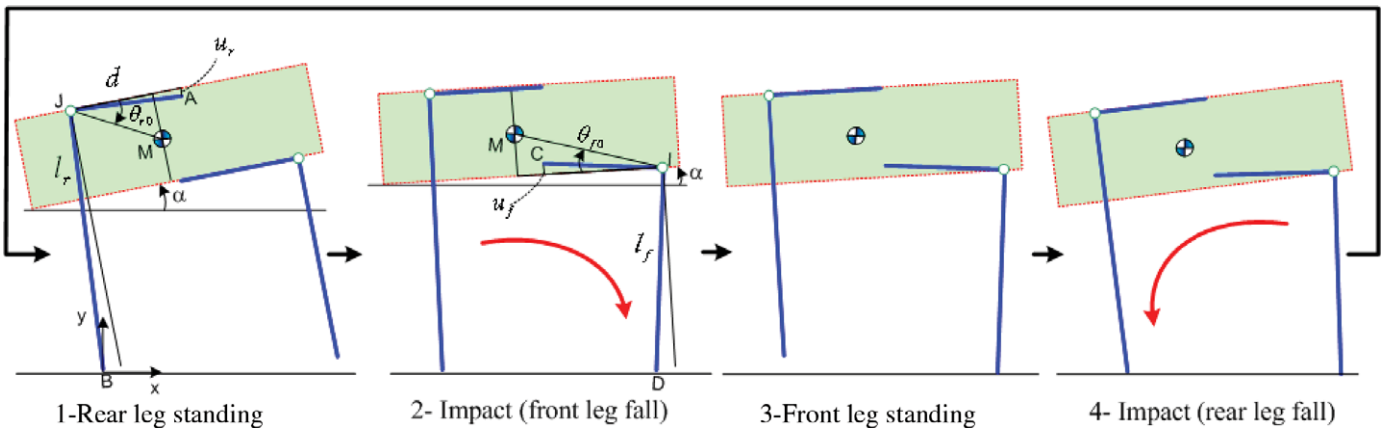

Fig. 5. (Colour online) Four phases of the bounding gait.

Here m is the robot weight and J_r is the moment of inertia of robot body around the rotation joint J. In this dynamics relationship, the input is the torque τ_r generated at the rear hip joint and the output is the rear leg angle and the robot body angle. By controlling the joint torque one can adjust the robot pose.

A similar approach can be taken for the dynamic analysis for the third phase called the front leg standing phase. The rear leg does not contact the floor and the robot body is supported by the front legs only. Due to the symmetric characteristics of the robot configuration, the dynamics model for the front leg standing phase can be derived similarly. The corresponding dynamics equations are shown in (2).

$$\begin{cases} ml_f^2\ddot{q}_1 + ml_f L_f \ddot{q}_2 \sin(q_1 - q_2) \\ \quad - ml_f L_f \dot{q}_2^2 \cos(q_1 - q_2) - mgl_f \sin q_1 = \tau_f \\ ml_f L_f \ddot{q}_1 \sin(q_1 - q_2) + (mL_f^2 + J_f)\ddot{q}_2 \\ \quad + ml_f L_f \dot{q}_1^2 \cos(q_1 - q_2) - mgL_f \cos q_2 = 0. \end{cases} \tag{2}$$

The second phase named the front leg falling phase follows the rear leg standing phase displayed in Fig. 5. It is noted that the collision time between the leg and the floor in the falling phase is very short. Although the external force (gravity) exists, the angular momentum change is negligible. In other words, the angular momentum of the system is conserved. In building the dynamics model for the falling phases, the superscript "−" indicates the moment before the collision between the leg and the floor and the "+" indicates the moment after the collision. The conservation equation of z component of angular momentum is $L^- = L^+$. The z component of angular momentum is computed by Eq. (3).

$$L = I\omega + m(x_{DM}\dot{y} - y_{DM}\dot{x}). \tag{3}$$

Here I is the moment of inertia of the robot body around z axis through the robot center, ω is the angular velocity of the robot body, i.e., $\omega = \dot{\alpha}$. The coordinates x_{DM} and y_{DM} are the position components of the robot center M with respect to the toe D (collision point) of the front leg. And $\dot{x}$, $\dot{y}$ are velocity components of the robot body in x and y directions, respectively. More derivation of the momentums L^- and L^+, the conservation equation is obtained in (4).

$$\begin{aligned} &I\dot{\alpha}^- + m\left[\left(-l_f \sin\left(\alpha + \frac{u_f}{d}\right) - L_f \cos(\alpha + \theta_{f0})\right)\dot{y}^-\right. \\ &\quad \left. - \left(l_f \cos\left(\alpha + \frac{u_f}{d}\right) - L_f \sin(\alpha + \theta_{f0})\right)\dot{x}^-\right] = \\ &I\dot{\alpha}^+ + m\left[\left(-l_f \sin\left(\alpha + \frac{u_f}{d}\right) - L_f \cos(\alpha + \theta_{f0})\right)\dot{y}^+\right. \\ &\quad \left. - \left(l_f \cos\left(\alpha + \frac{u_f}{d}\right) - L_f \sin(\alpha + \theta_{f0})\right)\dot{x}^+\right]. \end{aligned} \tag{4}$$

Equation (4) is called the front leg collision equation. Since the collision period is extremely short, the position parameters do not change during the collision and they are known ones. The velocities of the robot before the collision are also known. The unknown variables are velocities of the robot after the collision and Eq. (4) is used to compute them.

The fourth phase, the rear leg falling phase, follows the front leg standing phase. The last model in Fig. 5 shows the robot pose in this phase. Similarly the conservation of angular momentum $L^- = L^+$ can be obtained.

$$\begin{aligned} &I\dot{\alpha}^- + m\left[\left(-l_r \sin\left(\alpha + \frac{u_r}{d}\right) + L_r \cos(\alpha + \theta_{r0})\right)\dot{y}^-\right. \\ &\quad \left. - \left(l_r \cos\left(\alpha + \frac{u_r}{d}\right) - L_r \sin(\alpha + \theta_{r0})\right)\dot{x}^-\right] = \\ &I\dot{\alpha}^+ + m\left[\left(-l_r \sin\left(\alpha + \frac{u_r}{d}\right) + L_r \cos(\alpha + \theta_{r0})\right)\dot{y}^+\right. \\ &\quad \left. - \left(l_r \cos\left(\alpha + \frac{u_r}{d}\right) - L_r \sin(\alpha + \theta_{r0})\right)\dot{x}^+\right]. \end{aligned} \tag{5}$$

3.3. Direction control

Though our previous quadruped robot is a self-contained one with a decent speed [18], it has an inevitable weak point that stems from the characteristics of bounding gait: the robot cannot change the locomotion direction. Since the motion in the ideal bounding gait is symmetric, the robot is supposed to move straight all the time. Any change in the locomotion direction can occur as a result of noises and uncontrollable factors. Therefore, its application to useful missions should be limited.

https://doi.org/10.1017/S0263574712000112 Published online by Cambridge University Press

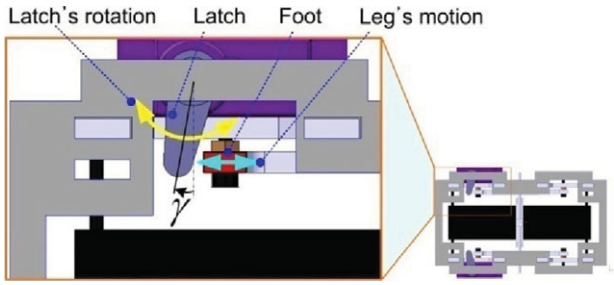

Fig. 6. (Colour online) Latch that constrains the motion of rear leg.

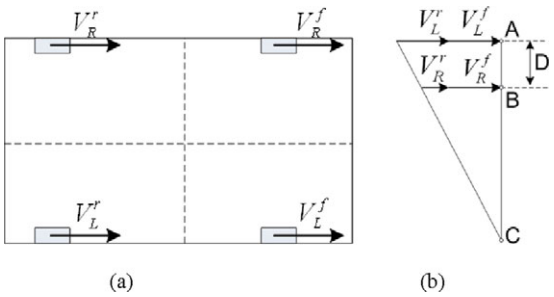

Fig. 7. (Colour online) Velocities of each side of the robot: (a) Velocities of each leg. (b) Formation of instantaneous center of rotation (viewed from bottom).

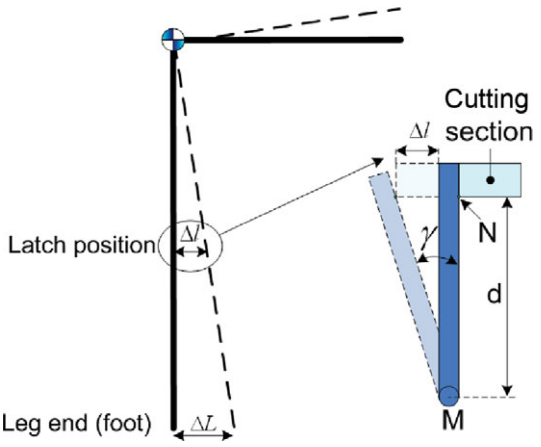

Fig. 8. (Colour online) Limited motion range of the leg when the latch device is activated.

Our proposed idea of direction control is to break the symmetry of the bounding gait. The solution in our robot is using two devices called latches. Two latches are moved by two RC-servo motors that are light and consume a small amount of power. The latches stop or constrain the motion of rear legs such that the rear legs move asymmetrically. As a result, the robot can change the locomotion direction. Figure 6 displays the installation of one RC-servo motor and the latch on the robot from the bottom side.

As shown in Fig. 6, the latch works like a barrier to the motion of the rear leg. When the robot performs a forward straight locomotion, the latch angle γ is opened to the maximum amount. There is no collision between the robot leg and the latch, and so the leg can move freely. If the robot needs to turn right, the right RC-servo motor makes the latch get closer to the rear leg, and thus the angle γ is reduced. Hence a collision between the rear leg and the latch occurs. If the angle γ is too small, the rear leg can be "locked," but otherwise the displacement range of the leg is reduced. The motion of left leg is larger than that of the right one, and hence the robot can make a right turn. A left turn can be realized in a similar way. This control method can be unsuccessful if the LIPCA is completely rigid. Since the two rear legs are actuated by one LIPCA, any interaction on one rear leg can have an effect on the other one. Fortunately, LIPCA has a sufficient flexibility to afford the control method.

For either straight-line locomotion or turning motion, the motion of each leg makes a contribution to the total motion of the robot. Using the principle of sum of velocity, one can consider that the velocity of each side of the robot in one vibration of legs as under:

$$\begin{cases} V_L = V_L^r + V_L^f \\ V_R = V_R^r + V_R^f. \end{cases} \tag{6}$$

The subscripts indicate the right and left sides and the superscripts are for the front and rear ones. Figure 7(a) displays the velocities of each leg.

Since the latches are attached at the rear legs only, activating the latches may change the average velocities of the rear legs. In the case of right turning for example, the right latch is activated to latch the right rear leg. Although the instantaneous velocities of two rear legs are equal, the constraint of the latch makes the average velocities can be different. The relations between average velocities are $V_L^r > V_R^r$ and $V_L^f = V_R^f$. As a result, the temporary center of rotation (TCR) is formed as shown in Fig. 7(b). Note in Fig. 7(b) that A and B are two end points of the legs on two sides of the robot and D is the distance between two sides.

One may have a question that since the front legs are symmetric and have the identical velocities, they may resist the turning motion produced by the rear legs. However, the situation does not happen to the bounding robot. As shown in phase 1 and phase 3 in Fig. 5, the rear legs and the front ones are activated alternately. While the rear legs push the ground to generate forward motion for the robot, the front legs are off the ground. Therefore, the front legs do not resist turning.

One can observe that even when the right rear leg is latched (but not locked) the leg still vibrates in the same frequency with other legs. However, the motion range of the end point of this leg is limited in the range of ΔL, which is smaller than its counterparts of other legs (see Fig. 8 for ΔL). The distance ΔL also corresponds to the velocity of the right rear leg, i.e., $V_R^r = \Delta L$.

The motion range ΔL is decided by the angle γ of the latch device. Figure 8 displays the side-view of the leg where the latch device is located at about the middle of the leg. The motion range ΔL therefore is related to the latch angle γ by the equation $\Delta L = 2\Delta l = 2d \tan\gamma$. The location of TCR can be derived from Fig. 7(b).

$$CA = \frac{D\left(V_L^r + V_L^f\right)}{V_L^r - \Delta L} = \frac{DV_L}{V_L^r - \Delta L}. \tag{7}$$

https://doi.org/10.1017/S0263574712000112 Published online by Cambridge University Press

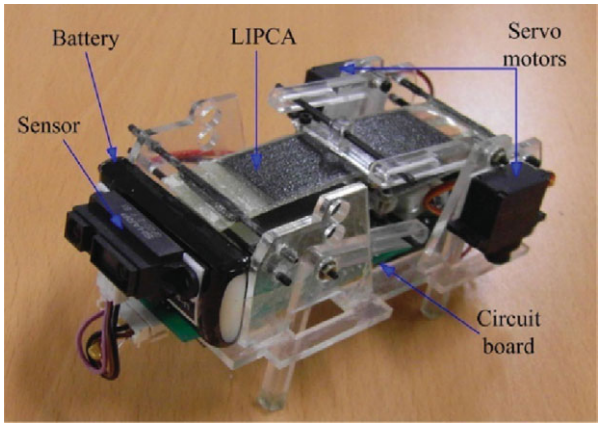

Fig. 9. (Colour online) Complete form of the bounding prototype with a circuit board and a battery on board.

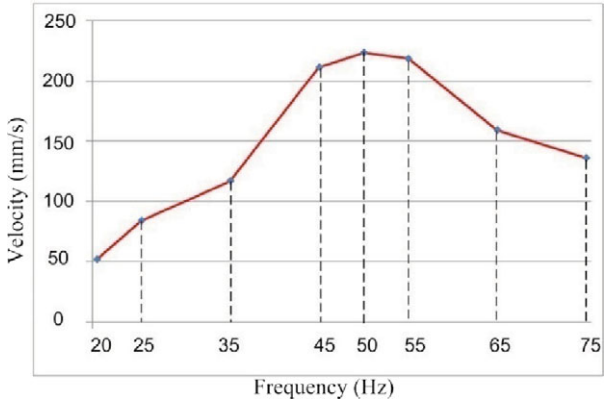

Fig. 10. (Colour online) Locomotion speed of the robot at different frequencies of applied voltage.

The rotation radius can be computed from TCR to the middle line of the robot body:

$$R = CA - \frac{D}{2} = \frac{DV_L}{V_L^r - \Delta L} - \frac{D}{2} = \frac{DV_L}{V_L^r - 2d\tan\gamma} - \frac{D}{2}. \tag{8}$$

It leads to an important feature of the direction control method: the rotation radius can be controlled by the value of latch angle γ (see experimental results in Section 4.2). It is verified by experiments that a pure rotation (rotation with very small radius) is also possible when one leg is locked and the other leg is free to move. This type of turning can be useful in situations where robots may fall, for example, when a robot walks in a narrow space.

4. Experimental Results and Discussion

4.1. Prototype

A bounding robot prototype has been fabricated based on the design in Section 2. The prototype is mostly made of acrylic. Each part was designed with AutoCAD and fabricated using a CNC machine. The robot frame was made by assembling the parts in the order. Two LIPCA pieces are connected to the robot frame with carbon rods and bearings are used at the rotation joins. The length, width, and height of the prototype are 120 mm, 80 mm, 70 mm, respectively. The weight of the robot is 70 g including the two RC-servo motors. The servo motor is digital HDS-877 RC-servo which is able to produce 1.2 kg.cm torque at 4.8 V supply. When the power supply and control circuit board is installed in the robot frame, the robot weight is increased to 135 g. The total weight of robot can vary depending on the type of battery on board. In fact the robot has been tested with several kinds of Li-Poly battery, whose weight is between 20 g and 55 g. Figure 9 shows the complete bounding prototype robot with a circuit board and an Apache Li-Poly battery on board.

4.2. Experiments and results

In order to evaluate the performance of the robot, four sets of experiments were conducted on a flat plywood panel of 1 m length, which is assumed to make no deformation during the robot's motion. All the experiments were performed with a 45 g, 800 mAh Li-Poly battery. The first set of experiments is for measuring the straight locomotion speed of the prototype at different frequencies of voltage that is applied to the LIPCA pieces. The RC-servo motors for the direction control are installed but deactivated in this experiment because the straight locomotion speed is the issue. The power supply and control board generates a square voltage signal to excite the LIPCA pieces. The amplitude of the voltage is fixed at 370 Vpp and the frequency is changed manually with switches on the board. Figure 10 shows the average speed of five trials versus the frequency of applied voltage.

The experimental results show that the maximum value of straight locomotion speed is about 220 mm/s when the frequency is 50 Hz. It is quite a remarkable result since it means that the robot can move about two times its body length per second with a heavy load (110 g of the circuit board and the battery combined). Compared to our previous robot [18], the locomotion speed has been improved by more than four times.

It is also noted that although the locomotion speeds at 25 Hz or 35 Hz are lower than the maximum speed, the robot is observed to move more stably at these frequencies. The robot maintains the locomotion direction better and the pitching level of robot body is smaller. The reason we get the highest speed of the robot at 50 Hz can be explained by that the resonance of the robot system is obtained at the frequency.

The second set of experiments is for ascertaining the direction control ability of the robot. The turning experiments verify the turning action of the robot in both principle and quantity. Through these experiments, the turning radius of the robot is measured and compared to theoretical values obtained from Eq. (6). In Eq. (6), D and q are design parameters, which are 38 mm and 7 mm, respectively. The velocities V_L and V_L^r are measured from experiments. They are in fact the vibration distances of the legs on the left side of the robot. It is shown in the first experiment set that the maximum velocity of the robot can be obtained when the driven frequency for LIPCA is about 50 Hz. However, the motion of the robot at this frequency is less unstable. Therefore, for the turning experiments, the

https://doi.org/10.1017/S0263574712000112 Published online by Cambridge University Press

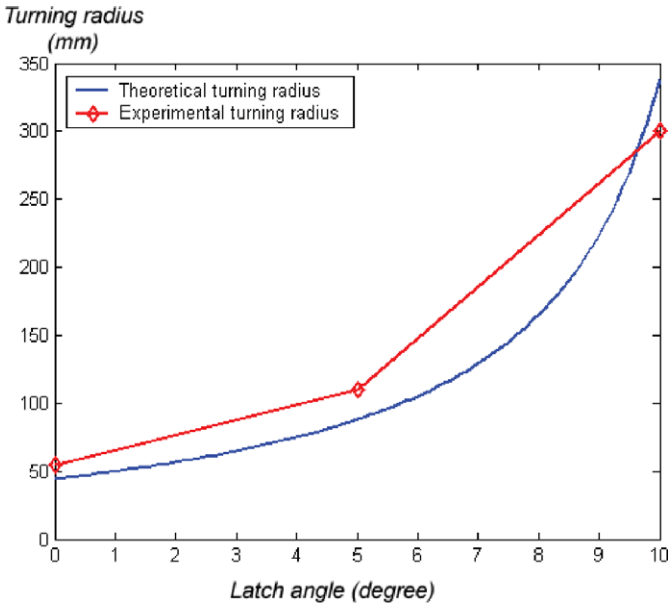

Fig. 11. (Colour online) Comparison of theoretical and experimental results on the turning radius versus latch angle.

operation frequency is set at 45 Hz. At this frequency, the robot speed is still high and the motion is stable. In this condition, the vibration distance of the rear leg and the front leg on the left side are about 3 mm and 2 mm. Therefore, the velocities in Eq. (6) are $V_L = V_L^r + V_L^f = 3 + 2 = 5 \quad mm/cycle$. The rotation radius for the 45 Hz operation frequency can be obtained from Eq. (8).

$$R = \frac{DV_L}{V_L^r - 2d\tan\gamma} - \frac{D}{2} = \frac{180}{3 - 14\tan\gamma} - 19.$$

Figure 11 shows the theoretical relation between the turning radius and the latched angle γ as well as the experimental results. A video that shows the straight-line locomotion and turning of the robot prototype can be found in the following online link: http://www.youtube.com/watch?v=cGvgo0KSsH0.

In the third experiment set for investigating the power consumption, the prototype robot is set free to run with 370 Vpp and 35 Hz frequency applied. We measured the total operation time of the robot until the battery ran out. With the 800 mAh Li-Poly battery onboard, the operation time was approximately 35 min, which results in a range of approximately 250 m. Compared to our previous robot [18], the power consumption has been improved by seven times, which provides larger chances for the robot to be used in useful missions.

As the final set of experiments, we checked the reliability of the robot in a critical circumstance where the two front legs are disabled due to the failure of the bottom LIPCA piece. The experiments were conducted in the same condition as the first set: the applied voltage at 370 Vpp and the frequency between 20 Hz and 50 Hz. It was found from the experiments that although the locomotion speed was reduced significantly, the robot was still able to maintain the ability of forward locomotion and turning with only two rear legs actuated. In case where the two rear legs were disabled, the robot was still capable of performing the forward locomotion. In this case, any turning could not be obtained because the servo motors that control the turning motion are installed in the rear legs. This feature can be quite a useful advantage that can elevate the reliability of the robot especially when the robot is assigned a mission in unknown environments.

4.3. Discussion

Compared to other legged robots that are actuated by unconventional actuators, our quadruped robot possesses several advantages. (See Table I for the features of six legged robots.) The most outstanding strength is the agility. Due to the simple structure and the symmetry based on the bounding gait, the robot is able to maintain the direction stably while moving with a high speed.

The agility is also attributed to the light weight of our robot. Thin and light piezocomposite actuator is an important factor in reducing the weight. The total weight of the robot is about 135 g, which includes the LIPCA actuators (4.8 g for each piece), the circuit board, and battery. Compared to the MERbot [13], which employs another type of unconventional actuator named electroelastomer roll actuator, our robot is about two times lighter.

Due to the limitation in the actuation force or displacement, robots actuated by unconventional actuators usually show the disadvantage in the locomotion speed. For example, the silicon micro-robot [25] can move at 0.4 times its body length per second. The speed parameter is 1 in case of the RoACH robot [12], and 2/3 for the MERbot. Note that the speed of RoACH is measured in the untethered mode but that of MERbot is measured when the power is supplied by an external power supply. However, our robot can move about two times its body length per second with the circuit and a battery on board.

If our robot is compared particularly to Goldfarb's quadruped robot [10] which employs piezoelectric actuators and the trotting gait, the most significant distinction can be found in the control method. In case of Goldfarb's robot, a frequency-based control method is used. The robot is able to turn right in the range of 14–18 Hz, move straight in 18–19 Hz, and turn left in 19–24 Hz. However, if the payload of the robot changes, the frequency ranges are shifted. Since the working range of frequency in this robot is narrow, the motion control can become unstable. On the contrary, our robot can operate in a wide range of applied frequency (from 20 Hz to 75 Hz). In addition, the direction control work is separated with the motion control, and hence the robot is able to perform both straight locomotion and turning in a various range of motion speed with a high stability. Another outstanding strength of our bounding robot is the ability to continue locomotion even when one of two LIPCA actuators fails. This feature is unique and important, considering that it may help the robot escape dangerous situations and continue its mission.

As shown in Table I, when our robot is compared to legged robots such as Sprawlita and RHex that use motors or pneumatic actuators, it shows a good speed and operation time with a smaller size and weight. Considering that small mobile robots are useful for application like monitoring and

https://doi.org/10.1017/S0263574712000112 Published online by Cambridge University Press

Table I. Comparison of legged mobile robots.

Robot	Actuator	Weight (kg)	Length (m)	Locomotion gait	Speed (length/sec)	Operation time (min)	Power source	Direction control method
Mesoscale legged robot [10]	Two PZT material actuators	0.037	0.09	Trotting	1.67	30	Battery on board	Frequency
MERbot [13]	Six electro elastomer rolls	0.292	0.18	Dual tripod	2/3	–	External supplier	–
RoACH [12]	Two SMA wires	0.0024	0.03	Walking	1	9	Self-contained	Leg length difference
Sprawlita [8]	Six servos and six pneumatic pistons	0.257	0.18	Walking, running	3	–	External supplier	–
RHex [9]	Six DC motors	7	0.53	Open-loop tripod gait	1	15	Self-contained	–
LIPCA bounding robot	Two LIPCA actuators and two servos	0.135	0.12	Bounding	2	35	Self-contained	Average velocity difference

exploration, out robot can be used as a mobile platform for such purposes.

5. Conclusion

We presented the implementation of a mesoscale, self-contained quadruped robot that is actuated by two pieces of piezocomposite actuator only. By introducing a simple but effective structure in the design of body and legs, the weaknesses in the LIPCA actuator displacement and insufficient number of DOF have been overcome significantly. The bounding gait was employed for the robot and it helped the robot improving the speed and maintaining the stability during the locomotion.

Two types of control in the locomotion were implemented to obtain the full motion ability: locomotion speed and direction. The locomotion speed of the robot can be changed by the frequency of applied voltage to the actuators. The highest speed can be obtained at 50 Hz, but about 40 % of the maximum speed is still attainable at 25 Hz. The heading direction of the robot can be changed by the turning motion, which is controlled by two RC-servo motors that are installed in the rear legs.

For the purpose of untethered robot, a power supply and control circuit board was developed and installed on the robot. The circuit board can supply a high voltage signal to excite the LIPCA actuators from a DC battery. Locomotion control algorithms can also be embedded in the microcontroller of the board. The robot can locomote continuously for 35 min with the board and a battery installed. Experiments with a prototype verify that the robot can perform the straight locomotion agilely and stably. It is also verified that the robot can turn by adjusting the latch angle parameter with the RC-servo motors.

Though several essential parts for developing a mesoscale autonomous quadruped robot driven by piezocomposite actuators have been achieved, there still remain significant pieces of work. Though servo motors take an important role for the direction control, their weight is relatively large. One of the candidates that we consider to replace the servos is shape memory alloy (SMA) wire. SMA wires are very lightweight but they can produce quite a large force when their shapes change [26]. They can be controlled by a low voltage electric source. Hence, we expect that they would be suitable for the direction control of the robot. A sensor system is planned to be added to the robot for avoiding obstacles and transmitting information. A stable gait planning and an autonomous navigation algorithm are also significant issues. Though various works including the landing accordance ratio method [27] have been reported, a novel approach needs to be considered because the legged robot employs unconventional actuators.

Acknowledgments

This work was supported by National Research Foundation of Korea Grant funded by the Korean Government (2009-0077778) and also supported by Leading Foreign Research Institutes Recruitment Program through the National Research Foundation of Korea funded by the Ministry of Education, Science and Technology (MEST) (2011-00260).

References

1. J. Estremera, E. Garcia and P. Gonzalez de Santos, "A multi-modal and collaborative human–machine interface for a walking robot," *J. Intell. Robot. Syst.* **35**, 397–425 (2002).
2. B. Klaassen, R. Linnemann, D. Spenneberg and F. Kirchner, "Biomimetic walking robot SCORPION: Control and modeling," *Robot. Auton. Syst.* **41**, 69–76 (2002).
3. P. Siegwart and I. R. Nourbakhsh, *Introduction to Autonomous Mobile Robots* (The MIT Press: Massachusetts, 2004).
4. P. Gonzalez de Santos, J. Estremera and E. Garcia, *Quadrupedal Locomotion: An Introduction to the Control of Four-legged Robots* (Springer: Germany, 2006).
5. D. A. Kingsley, R. D. Quinn and R. E. Ritzmann, "A Cockroach Inspired Robot with Artificial Muscles," **In**: *International Conference on Intelligent Robots and Systems*, Beijing (2006) pp. 1837–1842.
6. R. Playter, M. Buehler and M. Raibert, "BigDog," **In**: *Proceedings of the SPIE Defense and Security Symposia,*

https://doi.org/10.1017/S0263574712000112 Published online by Cambridge University Press

Unmanned Systems Technology, Orlando, vol. 6230, (2006) pp. 623020.
7. Y. Fukuoka and H. Kimura, "Dynamic locomotion of a biomorphic quadruped 'Tekken' robot using various gaits: Walk, trot, free-gait and bound," *Appl. Bionics Biomech.* **6**, 63–71 (2009).
8. S. A. Bailey, J. G. Cham, M. R. Cutkosky and R. J. Full, "Comparing the locomotion dynamics of the cockroach and a shape deposition manufactured biomimetic hexapod," *Experimental Robotics VII, Lecture Notes in Control and Information Sciences* **271**, 239–248 (2001).
9. U. Saranli, M. Buehler and D. E. Koditschek "RHex: A simple and highly mobile hexapod robot," *Int. J. Robot. Res.* **20**, 616–631 (2001).
10. M. Goldfarb, M. Gogola, G. Fischer and E. Garcia, "Development of a piezoelectrically-actuated mesoscale robot quadruped," *J. Micromechatronics* **1**, 205–219 (2001).
11. R. Sahai, S. Avadhanula, R. Groff, E. Steltz, R. Wood and R. S. Fearing, "Towards a 3g Crawling Robot through the Integration of Microrobot Technologies," **In**: *Proceedings of the International Conference on Robotics and Automation*, Orlando (2006) pp. 296–302.
12. A. M. Hoover, E. Steltz and R. S. Fearing, "RoACH: An Autonomous 2.4g Crawling Hexapod Robot," **In**: *Proceedings of International Conference on Intelligent Robots and Systems*, Nice, France (2008) pp. 26–33.
13. Q. Pei, M. Rosenthal, S. Stanford, H. Prahlad and R. Pelrine, "Multiple-degrees-of-freedom electroelastomer roll actuators," *Smart Mater. Struct.* **13**, N86–N92 (2004).
14. K. J. Yoon, S. Shin, H. C. Park and N. S. Goo, "Design and manufacture of a lightweight piezo-composite curved actuator," *Smart Mater. Struct.* **11**, 163 (2002).
15. K. Y. Kim, K. H. Park, H. C. Park, N. S. Goo and K. J. Yoon, "Performance evaluation of lightweight piezo-composite actuators," *Sensor. Actuat. A: Phys.* **120**, 123–129 (2005).
16. K. J. Yoon, K. H. Park, S. K. Lee, N. S. Goo and H. C. Park, "Analytical design model for a piezo-composite unimorph actuator and its verification using lightweight piezo-composite curved actuators," *Smart Mater. Struct.* **13**, 459–467 (2004).
17. K. M. Mossi and R. P. Bishop, "Characterization of Different Types of High Performance THUNDER Actuators," **In**: *Proceedings of theSPIE Conference*, Newport Beach, CA, vol. 3675, (Mar. 1999) pp. 43–52.
18. T. Ho and S. Lee, "Piezoelectrically actuated biomimetic self-contained quadruped bounding robot," *J. Bionic Eng.* **6**, 29–36 (2009).
19. E. Steltz, M. Seeman, S. Avadhanula and R. S. Fearing, "Power Electronics Design Choice for Piezoelectric Microrobots," **In**: *Proceedings of the International Conferenceon Intelligent Robots and Systems*, Beijing, China (2006) pp. 1322–1328.
20. I. Poulakakis, J. A. Smith and M. Buehler, "Modeling and experiments of untethered quadrupedal running with a bounding gait: The scout II robot," *Int. J. Rob. Res.* **24**, 239–256 (2005).
21. M. Buehler, A. Cocosco, K. Yamazaki and R. Battaglia, "Stable Open Loop Walking in Quadruped Robots with Stick Legs," **In**: *Proceedings of the International Conference on Robotics and Automation*, Detroit, Michigan, vol. 3 (1999) pp. 2348–2353.
22. Y. Zhou, "On the planar stability of rigid-link binary walking robots," *Robotica* **21**, 667–675 (2003).
23. T. Ho and S. Lee, "Two Types of Biologically-Inspired Mesoscale Quadruped Robots," **In**: *Proceedings of the International Conference on Robotics, Automation and Mechatronics*, Chengdu, China (2008) pp. 1148–1153.
24. J. Furusho, A. Sano, M. Sakaguchi and E. Koizumi, "Realization of Bounce Gait in a Quadruped Robot with Articular-Joint-Type Legs," *Proceedings of The IEEE International Conference on Robotics and Automation,* Nagoya, Japan (1995) pp. 697–702.
25. T. Ebefors, J. U. Mattsson, E. Kälvesten and G. Stemme, "A Walking Silicon Micro-Robot," **In**: *Proceedings of the 10th International Conference on Solid-State Sensors and Actuators*, Sendai, Japan (1999) pp. 1202–1205.
26. C. Mavroidis, "Development of advanced actuators using shape memory alloys and electrorheological fluids," *Res. Nondestruct. Eval.* **14**, 1–32 (2002).
27. M. Won, T. H. Kang and W. K. Chung, "Gait planning for quadruped robot based on dynamic stability: Landing accordance ratio," *Intell. Serv. Robot.* **2**, 105–112 (2009).

https://doi.org/10.1017/S0263574712000112 Published online by Cambridge University Press